WIND ENERGY
Wind Energ. 2017; **00**:1–18
DOI: 10.1002/we

RESEARCH ARTICLE

Gridded Based LPV Control of A Clipper Liberty Wind Turbine

Shu Wang and Peter Seiler

Aerospace Engineering and Mechanics, University of Minnesota, Minneapolis, MN, USA

ABSTRACT

This paper proposes a linear parameter varying (LPV) control design for a Clipper Liberty C96 2.5 MW wind turbine to operate in all wind conditions. A standard approach is to use multiple single-input, single-output (SISO) loops for control objectives at different wind speeds. This LPV controller instead takes these objectives into a uniformed multi-input, multi-output (MIMO) design framework. The key difference is that the LPV controller is specifically designed to smoothly transition from Region 2 to Region 3 operation. Reducing structural loads is another major concern in the design. Synthesis of the controller relies on a gridded based LPV model of the turbine, which is constructed by interpolation of linearized turbine models at different wind speeds. To overcome the conservativeness in the design, parameter varying rates will be considered based on turbulent wind conditions. The performance of the LPV controller is evaluated using a high fidelity FAST model provided by Clipper. The LPV controller is directly compared against the baseline controller currently operating on the turbine. Simulations and analysis show that the LPV controller meets all performance objectives and has better load reduction performance.

KEYWORDS
Wind Turbine Control; Load Reduction; LPV Control

Received . . .

1. INTRODUCTION

Modern utility scale wind turbines are nonlinear multi-input, multi-output (MIMO) systems with distinct objectives in different wind conditions. Specifically, the turbine is operated to maximize the power generation in Region 2 and track the rated generator speed in Region 3 [1]. A classical baseline controller [2] uses two independent control loops for objectives in the two regions and ensure a smooth transition when the wind condition changes. As the turbine size grows and the structural dynamics become more flexible, considerations on load reduction are more critical [3, 4]. Therefore, extra control loops were proposed to reduce the structural loads, such as individual pitch control [5, 6, 7, 8, 9] and tower and drive train dampers [4, 10, 11, 12]. These methods significantly decreased the loads but lead more complicated control structures. There are also other concerns, such as performance degradation due to dynamic variations with the wind speed and potential dynamic couplings between control loops. An alternative approach is to consider multiple objectives into a systematic MIMO design [13]. This approach has been adopted in some papers and shown better potentials than the multiple SISO loops design [14, 15, 16].

This paper proposes a MIMO design for the Clipper Liberty C96 turbine using linear parameter varying (LPV) control. Theories on LPV systems and control have been developed over the past few decades [17, 18, 19] and verified in various applications [20]. It is promising to apply LPV control on wind turbines, as it is essentially developed for MIMO control purposes. Therefore, existing results on SISO control can be integrated into a uniform structure. Moreover, LPV control takes dynamic variations into consideration. In wind turbine applications, it is expected to achieve multiple objectives and ensure uniform performance and smooth transitions when the dynamics varies with the wind speed. For these reasons, LPV control is an interesting topic in the field of wind energy [21, 14, 22, 23, 24, 25, 26, 16, 11].

Existing results on this topic can be first categorized by their objectives. For instance, LPV control is used in [11] for generator speed tracking. The control system also contains additional loops for tower loads mitigation. In [16], an LPV controller is synthesized to improve the load reduction performance in Region 3 and an extra anti-windup LPV design in Region 2.5 is used to ensure bumpless transfer to Region 2. In [9], an LPV individual blade pitch controller is proposed

for reducing loads on blades and nacelle. LPV control has also been investigated for fault tolerant control of wind turbines [27]. Other related work include LPV model reductions [28] and integrated designs for structural and control improvements [29]. The most relevant prior work is [14] and [23]. In these papers, an LPV design is proposed that covers all regions and parameter varying weighting functions are included for multi-objectives.

These results can be further categorized by their modeling and design methods. Traditionally, there are two approaches to model LPV systems. In the first approach, state matrices of LPV models have a rational dependence on scheduling parameters [17, 30]. The control synthesis for these so called linear fractional transformation (LFT) based LPV system has been developed in [31, 17] and lead to finite dimensional linear matrix inequalities (LMIs). Related designs for wind turbines can be found in [21, 11]. Another group of LPV systems are called gridded based LPV systems [18, 19]. State matrices of these LPV systems have an arbitrary dependence on scheduling parameters. They are usually derived by linearization of nonlinear models and are more general in applications due to the assumption of the arbitrary dependence. However, the control synthesis leads to parameter-dependent LMIs [18, 19]. A remedy to this problem is to approximate the LPV system with LTI models on a finite gridding set of scheduling parameters. Wind turbine control designs using this approach can be found in [21, 22, 23, 24, 16].

It should be noted that the LPV control as described here is different from the common gain scheduling technique. Straight gain scheduling of controllers is widely used in practice and usually has an acceptable performance. However, there is no theoretical guarantee for performance, or even stability. This is because the gain scheduling technique neglects dynamics variations of the plant associated with the scheduling parameter. For an LPV model of the wind turbine that covers all wind speed regions, a gain-scheduled controller might not even be able to stabilize the plant.

In this paper, an LPV control design that covers all wind conditions is proposed for a Clipper Liberty C96 $2.5\,\mathrm{MW}$ wind turbine. This design is based on a high fidelity FAST model [32] of the turbine provided by Clipper. Specifically, a gridded based LPV model is constructed by interpolation of linearized turbine models at different wind speeds. Details of the Clipper turbine and the construction of the LPV model are described in Section 2 and 3, respectively.

The proposed LPV controller is able to maximize the power generation in Region 2 and track the rated generator speed in Region 3, similar to a classical baseline controller. Load reduction is another important part of the design. In fact, the use of MIMO control architecture for multi-objectives in an integrated design naturally ensures stability and performance at different wind speeds. The design procedure is therefore simplified and potential side effects due to the dynamics coupling and transition between SISO loops can be avoided. Compared to similar designs in [14] and [23], this paper has been extended in several aspects. First, more dynamic weighting functions are included for better loop shaping. Second, bounded parameter varying rates are considered to overcome the conservativeness in control synthesis. Third, the use of recently developed LPV toolbox [33] for synthesis is expected to improve the numerical stability and accuracy. Fourth, the controller has been designed and benchmarked against models and controllers of a full-scale turbine obtained from Clipper. Details of the LPV design will be presented in Section 4.

In Section 5, the LPV controller is compared with a baseline controller in FAST simulations. This baseline controller is also provided by Clipper and currently operates on the turbine. Simulation results show that the LPV controller operates the turbine similar to the baseline controller. The most attractive improvement for the LPV design is that turbine structural loads on the tower and high speed shaft have been significantly decreased, especially in Region 3. A brief conclusion of this paper and the future work is made in Section 6.

2. CLIPPER LIBERTY C96 WIND TURBINE

The model to be studied in this paper is the Clipper Liberty C96 wind turbine. This turbine, shown in Figure 1, is installed at the University of Minnesota UMore Park campus. This is an utility-scale wind turbine with a rated power of $2.5\,\mathrm{MW}$. It is owned by the EOLOS Wind Energy Research Consortium at University of Minnesota [34] for research purposes. Basics of the turbine are shown in Table I.

Table I. Basics of the C96 2.5 MW wind turbine.

Hub height	$80.4\,\mathrm{m}$
Rotor radius	$48\,\mathrm{m}$
Wind speed range for operation	$4 \sim 25\,\mathrm{m/s}$
Rated generator speed	$1133\,\mathrm{RPM}$
Rated generator torque	$23473\,\mathrm{N\cdot m}$
Rated power	$2.5\,\mathrm{MW}$

The C96 power curve, shown in Figure 2, has the standard operating regions. A mode-dependent baseline controller with distinct objectives [3, 35, 2] is used here. Below the cut-in speed of $4\,\mathrm{m/s}$ (Region 1), the turbine is shut down as

Wind Energ. 2017; **00**:1–18 © 2017 John Wiley & Sons, Ltd.
DOI: 10.1002/we
Prepared using weauth.cls

Figure 1. Clipper Liberty C96 2.5 MW wind turbine at University of Minnesota [34].

there is insufficient energy from the wind. From $4\,\mathrm{m/s}$ to $9\,\mathrm{m/s}$ (Region 2), the objective is to maximize the captured power. A standard $k\omega^2$ law is used to control the generator torque. From $9\,\mathrm{m/s}$ to $12\,\mathrm{m/s}$, Region 2.5 is introduced as a transition between Region 2 and Region 3. In this region, the collective blade pitch is used to track the rated generator speed and the generator torque keeps increasing until the wind speed reaches $12\,\mathrm{m/s}$. Between the rated and cut-out wind speeds (Region 3), the objective is to maintain the rated power. Only collective blade pitch is controlled to track the rated generator speed. A PI pitch controller is used for both Region 2.5 and Region 3. Above the cut-out speed of $25\,\mathrm{m/s}$ (Region 4), the turbine is shut down to prevent structural damages. It is noted that this baseline controller only relies on the measurement of generator speed and it does not contains any other loops for the tower or drive train damper.

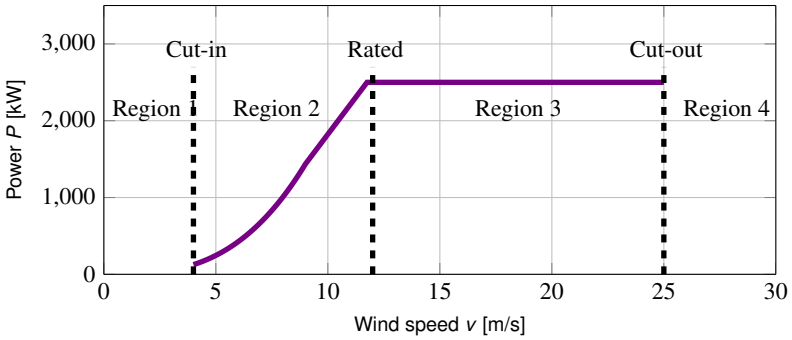

Figure 2. Operation regions for the C96 2.5 MW wind turbine.

For protection of intellectual properties, the detailed structure and parameters of the baseline controller will not be shown. However, similar designs can be found in [3, 35, 2]. It is noted that the baseline C96 controller includes low pass filters in both the blade pitch and generator torque loops. These filters limit the control bandwidth thus impacting the structural load reduction.

3. MODEL CONSTRUCTION

A high fidelity nonlinear model of the C96 turbine in FAST [32] is provided by Clipper. FAST can linearize the model at specified trim wind conditions. The linearization yields a periodic, linear time varying (PLTV) system due to the rotor/blade rotation. A "weakly" PLTV system is obtained using the Multi-Blade Coordinate (MBC) transformation followed by averaging the state matrices [36]. This process yields an LTI model with sufficient accuracy.

The proposed control design requires an LPV model of the turbine that captures dynamic variations with the wind speed. Therefore, this LPV model is dependent on the trim wind speed v_{trim} that varies from $4\,\mathrm{m/s}$ to $25\,\mathrm{m/s}$. In practice, a finite gridding set of v_{trim} is taken over the range [19] and the LPV model is constructed by linear interpolation of LTI models at the gridding set. To balance accuracy and complexity, here, 7 points are chosen uniformly in increments of $3\,\mathrm{m/s}$, from $6\,\mathrm{m/s}$ to $24\,\mathrm{m/s}$. For simplicity, the model below $6\,\mathrm{m/s}$ is represented by the LTI model at $6\,\mathrm{m/s}$ without extrapolation. Similar approximation is applied when v_{trim} is above $24\,\mathrm{m/s}$. Once a specific v_{trim} is selected, trim values for the generator

power, generator speed ω_{g_trim}, generator torque τ_{g_trim} and collective blade pitch angle β_{trim} can be determined uniquely. Figure 3 shows these trim values as functions of v_{trim}.

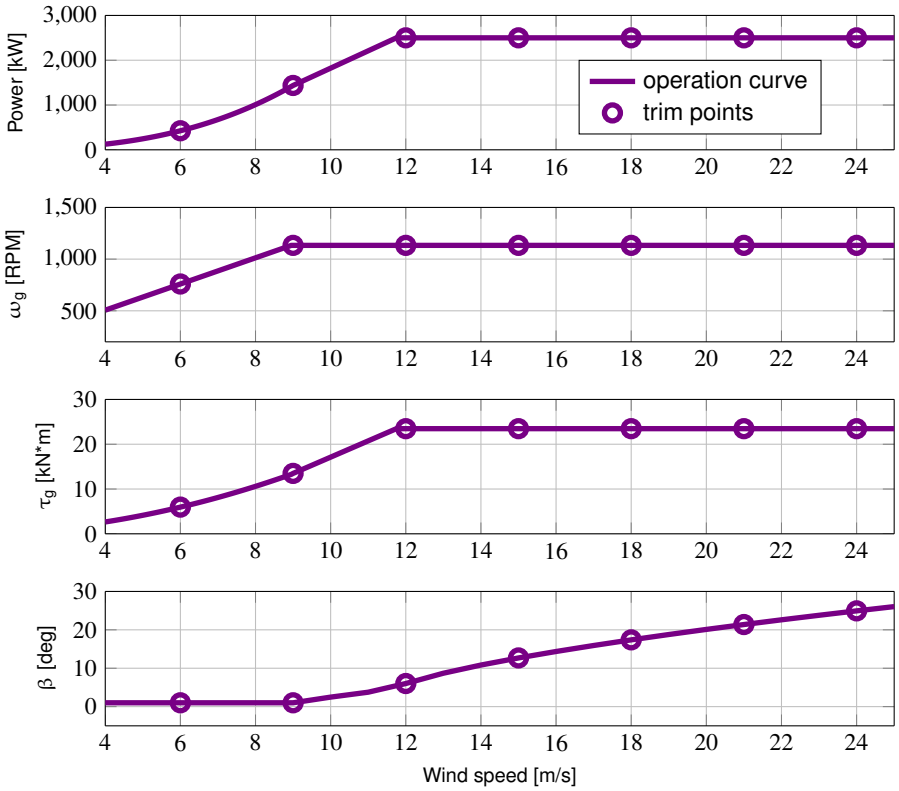

Figure 3. Trim values for linearization.

The FAST model here uses 9 degree of freedoms (DOFs) for linearization, which include the rotor position, first tower fore-aft and side-to-side bending modes, and first flapwise and edgewise bending modes for each blade. The linearized model therefore contains 18 states [32]. To avoid numerical issues, the state of rotor position is removed. It is noted that DOF of the drive train is usually included for damping vibrations on the rotor shaft. However, the C96 turbine has a rigid shaft such that the corresponding mode is at $178\,\mathrm{rad/s}$. This is far beyond the bandwidth of actuators and the wind turbulence has minor effects at this frequency. Therefore, it is reasonable to exclude this DOF from the model. For the C96 turbine, vibrations on the drive train are mainly induced by one of the blade edgewise bending modes after MBC. This mode is at about $13\,rad/s$ and the proposed design in this paper will be able to damp it. More importantly, this design should be transferable to other turbines for suppressing the drive train mode when the shaft stiffness is low and the induced load can not be neglected.

Control inputs to the model include generator torque $\delta\tau_g$ and collective pitch angle $\delta\beta$. The notation δ is used to indicate the difference between real value and trim value, which is commonly seen in linearization. The disturbance δv is the difference between hub height wind speed and trim wind speed, which captures characteristics of the turbulence. To penalize tower loads, tower fore-aft and side-to-side bending moments δM_{tfa} and δM_{tss} are selected as error outputs. However, δM_{tfa} and δM_{tss} are only incorporated in the model for control design and not required for controller implementation. This is in contrast to tower damper designs in [4, 10, 11, 12, 14, 23]. The only sensor measurement for feedback control is generator speed ω_g.

To conclude, the LPV model of the turbine $G(\rho)$ is given by the following form

$$\begin{bmatrix} \dot{x} \\ e \\ y \end{bmatrix} = \begin{bmatrix} A(\rho) & B_d(\rho) & B_u(\rho) \\ C_e(\rho) & D_{ed}(\rho) & D_{eu}(\rho) \\ C_y(\rho) & D_{yd}(\rho) & D_{yu}(\rho) \end{bmatrix} \begin{bmatrix} x \\ d \\ u \end{bmatrix} \tag{1}$$

where $x \in \mathbb{R}^{17}$ is the state, $d := \delta v \in \mathbb{R}$ is the disturbance, $u := \begin{bmatrix} \delta\tau_g & \delta\beta \end{bmatrix}^T \in \mathbb{R}^2$ is the vector of inputs, $e := \begin{bmatrix} \delta M_{tfa} & \delta M_{tss} \end{bmatrix}^T \in \mathbb{R}^2$ is the vector of error outputs and $y := \delta\omega_g \in \mathbb{R}$ is the sensor measurement. It is important to emphasize that state matrices of this model have an arbitrary dependence on $\rho := v_{trim}$ due to linearizations in FAST.

Wind Energ. 2017; **00**:1–18 © 2017 John Wiley & Sons, Ltd.
DOI: 10.1002/we
Prepared using weauth.cls

4. LPV CONTROL DESIGN

4.1. Overview of The LPV Controller

This section provides an overview of the proposed LPV controller for multiple performance objectives. This LPV controller, shown in Figure 4, has a dependence on $\rho := v_{trim}$. To get the measurement of v_{trim}, an estimate of the effective wind speed $\hat{v}$ can be constructed [37]. Alternatively, the wind speed measurement can be obtained from a LIDAR [38]. In either case, the wind speed fluctuates due to turbulence and hence low-pass filtering, denoted 'LPF' in the figure, is used to generate v_{trim}. It is noted that steady state values $\tau_{g\_trim}(\rho)$ and $\beta_{\_trim}(\rho)$ set up nominal operation conditions of wind turbine. For an LPV controller, these variables are dependent on ρ and therefore time varying. Here, the bandwidth of the LPF is $0.04\,rad/s$ such that ρ varies fast enough to capture the effective wind speed and slow enough to avoid exciting any structural modes through $\tau_{g\_trim}(\rho)$ and $\beta_{\_trim}(\rho)$. Therefore, the steady state values are expected to have minor side effects to the system performance.

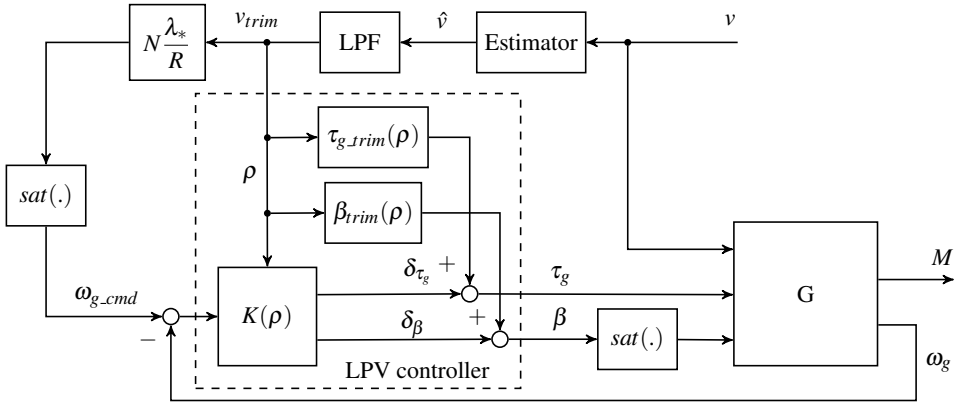

Figure 4. Structure of the LPV controller.

This controller will be designed to operate the turbine in all wind conditions. Specifically, in Region 2, the controller tracks a time varying command ω_{g_cmd} for maximizing the power generation. ω_{g_cmd} is calculated by the following equation:

$$\omega_{g\_cmd} = min\{N\frac{\lambda_*}{R}v_{trim},\, \omega_{g\_rated}\}, \tag{2}$$

where N is the gear box ratio, λ_* is the optimal tip speed ratio (TSR) [39] and R is the radius of the rotor. It it noted that $\omega_{g\_cmd} < \omega_{g\_rated}$ in Region 2. In this case, τ_g will be the main control actuation, such that the real time TSR tracks λ_*. The blade pitch actuation needs to be suppressed such that β is close to the optimal value β_* [39]. Therefore, the optimal power coefficient C_{p*} can be achieved [39]. A saturation block is used to prevent the pitch angle from dropping below β_*. In fact, $\frac{\partial C_p}{\partial \beta}$ is close to 0 when C_p is close to C_{p*} [40]. If λ_* can be well tracked, it is expected that the blade pitch actuation would have minor effects to the power generation.

It should be noted that this control strategy for Region 2 is different from the $k\omega^2$ law used in the baseline controller. However, it provides a consistent structure for operation above the rated wind. As shown in Equation 2, ω_{g_cmd} will be saturated at the rated value ω_{g_rated} when v_{trim} goes high. In this case, the control system looks similar to the baseline controller in Region 3. However, both τ_g and β will be actuated. β will be the main control input for maintaining the rated power and reducing the structural loads. τ_g will serve as a complementary control input for alleviating the usage of blade pitching on load reductions. This is based on the observation that both the two actuations have significant impacts on critical structural modes. As a example, Figure 5 shows the open loop frequency response from $\delta\tau_g$ and $\delta\beta$ to tower loads δM_{tfa} and δM_{tss} at $\rho = 18\,m/s$. It is noted that the objective for tower loads reduction will be achieved by directly penalizing the tower bending moments. As mentioned in Section 3, this is different from the tower damper designs [4, 10, 11, 14, 23], which are expected to have better performance, at the expenses of extra sensors and control complexity. The proposed LPV architecture here is able to incorporate the damper in the future, if further load reduction is required.

To summarize, the proposed control architecture is able to realize multiple objectives in a uniformed design. These objectives are listed below to guide the controller tuning process, which will be fully described in Section 4.2:

1. Track the optimal generator speed command $\omega_{g\_cmd}\,(:= N\frac{\lambda_*}{R}v_{trim})$ and capture at least 98 % of the power generated by the baseline controller in Region 2.

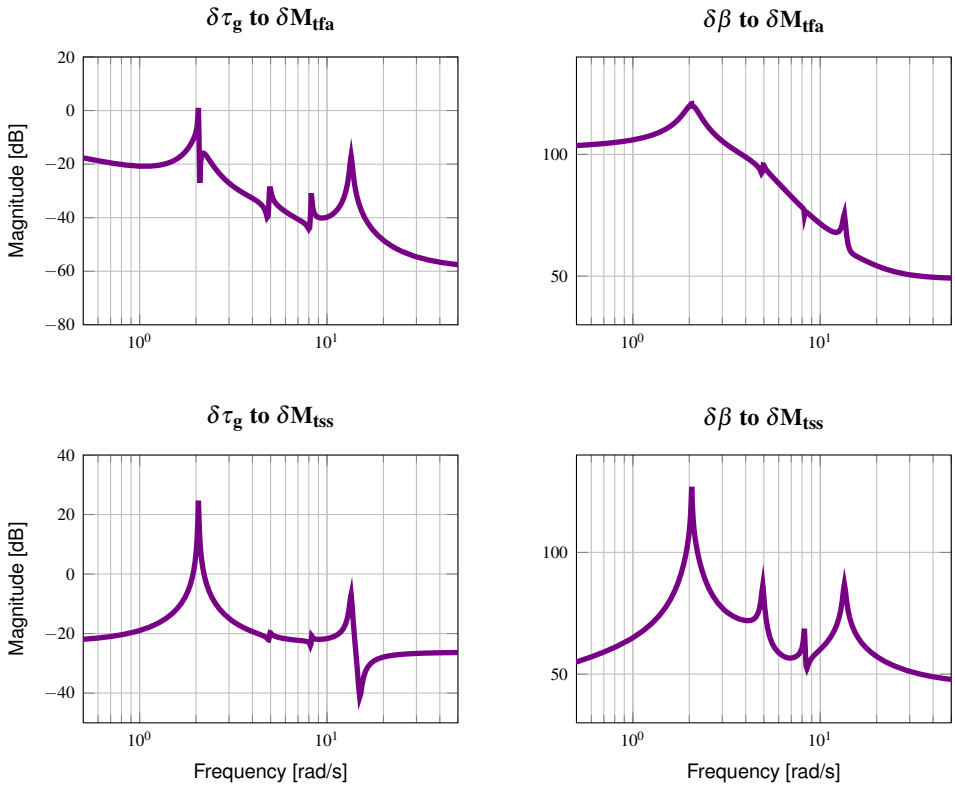

Figure 5. Open loop frequency responses at $\rho = 18 m/s$.

2. Track the rated generator speed ω_{g_rated} in Region 3 such that the standard deviation of tracking error is below $30 RPM$.
3. Ensure a stable and smooth transition in Region 2.5.
4. Reduce damage equivalent loads (DELs) [41] on the tower fore-aft bending moment M_{tfa}, side-to-side bending moment M_{tss} and the high speed shaft torque τ_{hss} by around 10% in Region 3..
5. Limit the blade pitch actuation beyond critical structural modes.

4.2. Tuning of Design Weights

Given the LPV model $G(\rho)$, shown in Figure 6(a), the goal is to synthesize an LPV controller $K(\rho,\dot{\rho})$ of the form:

$$\begin{bmatrix} \dot{x}_K \\ u \end{bmatrix} = \begin{bmatrix} A_K(\rho,\dot{\rho}) & B_K(\rho,\dot{\rho}) \\ C_K(\rho,\dot{\rho}) & D_K(\rho,\dot{\rho}) \end{bmatrix} \begin{bmatrix} x_K \\ y \end{bmatrix}. \tag{3}$$

The controller $K(\rho,\dot{\rho})$ generates the control input $u := [\,\delta\tau_g \;\; \delta\beta\,]^T$ based on the measurement $y := \delta\omega_e$. Design objectives as listed in Section 4.1 are specified by weighting functions W_e, W_τ, W_β, W_v and W_m, as shown in Figure 6(a). It is noted that there is an extra filter F_τ applied to the torque input channel to further limit low frequency actuation in Region 3. The interconnection of $G(\rho)$, F_τ and these weights is denoted by an augmented system $\tilde{G}(\rho)$, as shown in Figure 6(b). The closed-loop interconnection of $\tilde{G}(\rho)$ and $K(\rho,\dot{\rho})$ is given by a lower LFT and is denoted $\mathscr{F}_l(\tilde{G}(\rho),K(\rho,\dot{\rho}))$ [42]. The objective is to minimize the induced L_2 gain from $\tilde{d}$ to $\tilde{e}$:

$$\min_{K(\rho,\dot{\rho})} \left\| \mathscr{F}_l(\tilde{G}(\rho),K(\rho,\dot{\rho}) \right\|, \tag{4}$$

where $\tilde{d} := [\,\delta\bar{v} \;\; \delta\omega_{g\_cmd}\,]^T$ is the weighted disturbance and $\tilde{e} := [\,\delta\bar{\omega}_e \;\; \delta\tilde{\tau}_g \;\; \delta\tilde{\beta} \;\; \delta\tilde{M}_{tfa} \;\; \delta\tilde{M}_{tss}\,]^T$ contains all weighted errors.

This section provides details on how to tune F_τ and weighting functions for synthesizing the controller. For simplicity, they will all be called "design weights". However, it should be noted that F_τ will be implemented as part of the controller while all other weights are only used for loop-shaping.

Wind Energ. 2017; **00**:1–18 © 2017 John Wiley & Sons, Ltd.
DOI: 10.1002/we
Prepared using weauth.cls

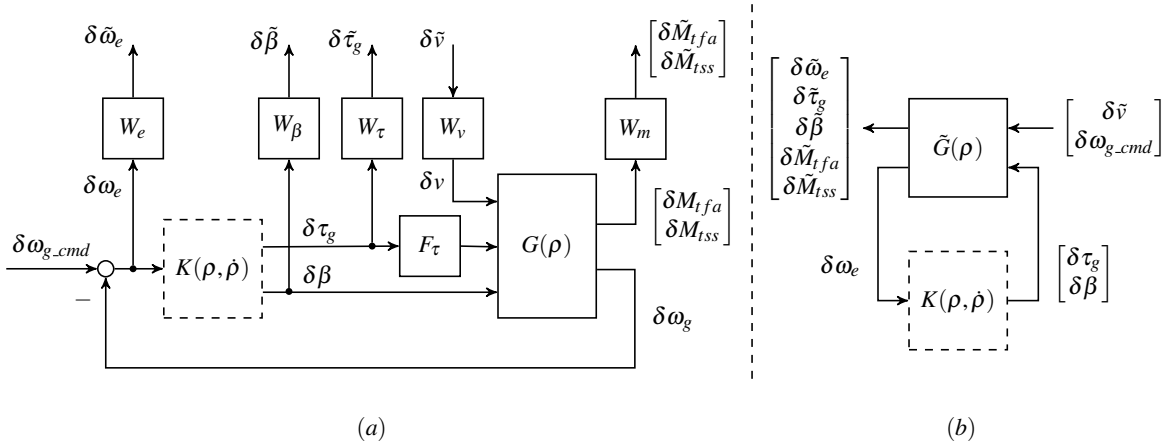

Figure 6. The augmented system for LPV synthesis (a) and the equivalent LFT transformation (b).

In general, LPV systems do not have a valid frequency domain interpretation. However, the frequency response at fixed (parameter) conditions exists, which allows classical loop-shaping techniques to be adapted. Specifically, performance objectives can be specified by design weights in the frequency domain. The freedom for tuning is even extended for LPV systems, as weights could also be linear parameter varying for distinct objectives at different trim points.

Table II shows expressions of these weights with respect to the trim points. Bode magnitude plots are provided in Figure 7 for $W_e^{(i)}$, $W_\tau^{(i)}$, $W_\beta^{(i)}$, $W_v^{(i)}$ and $F_\tau^{(i)}$ $(i = 1,...,4)$. The first group of weights (denoted as $W_e^{(1)}$, $W_\tau^{(1)}$, $W_\beta^{(1)}$, $W_v^{(1)}$, $W_m^{(1)}$ and $F_\tau^{(1)}$) is used for $\rho = 6\,\mathrm{m/s}$ and the second group is for $\rho = 9\,\mathrm{m/s}$. Objectives for Region 2.5 are specified by the third group of weights, which corresponds to $\rho = 12\,\mathrm{m/s}$. The last group of weights is chosen for Region 3, which correspond to ρ varying from $15\,\mathrm{m/s}$ to $24\,\mathrm{m/s}$.

Table II. Design weights at different trim points.

i	1	2	3	4
ρ	$[6]$	$[9]$	$[12]$	$[15\ 18\ 21\ 24]$
W_e	$0.15\dfrac{0.9091s+0.04333}{s+0.039}$	$0.15\dfrac{0.9091s+0.04333}{s+0.039}$	$0.2\dfrac{s+0.1192}{1.1s+0.08341}$	$0.15\dfrac{s+0.1192}{1.1s+0.04767}$
W_τ	$0.003\dfrac{s+0.3}{0.01s+0.3}$	$0.0012\dfrac{s+3}{0.01s+3}$	$0.005\dfrac{s+3}{0.05s+3}$	$0.008\dfrac{s+5}{0.05s+5}$
W_β	$30\dfrac{2.646s+1}{0.05292s+2}$	$30\dfrac{2.646s+1}{0.05292s+2}$	$25\dfrac{2.646s+2}{0.05292s+4}$	$10\dfrac{2.646s+6}{0.05292s+12}$
W_v	$0.4\dfrac{22.61s+15}{180.8s+240}$	$0.4\dfrac{22.61s+15}{180.8s+240}$	$0.4\dfrac{22.61s+15}{180.8s+240}$	$0.7\dfrac{14.11s+15}{84.64s+150}$
W_m	$\begin{bmatrix}10^{-3.65} & 0\\ 0 & 10^{-3.25}\end{bmatrix}$	$\begin{bmatrix}10^{-3.65} & 0\\ 0 & 10^{-3.25}\end{bmatrix}$	$\begin{bmatrix}10^{-3.65} & 0\\ 0 & 10^{-3.25}\end{bmatrix}$	$\begin{bmatrix}10^{-3.65} & 0\\ 0 & 10^{-3.25}\end{bmatrix}$
F_τ	$\dfrac{s+0.01459}{s+0.0175}$	$\dfrac{s+0.01459}{s+0.0175}$	$\dfrac{s+0.0378}{s+0.07559}$	$\dfrac{s+0.0898}{s+0.3592}$

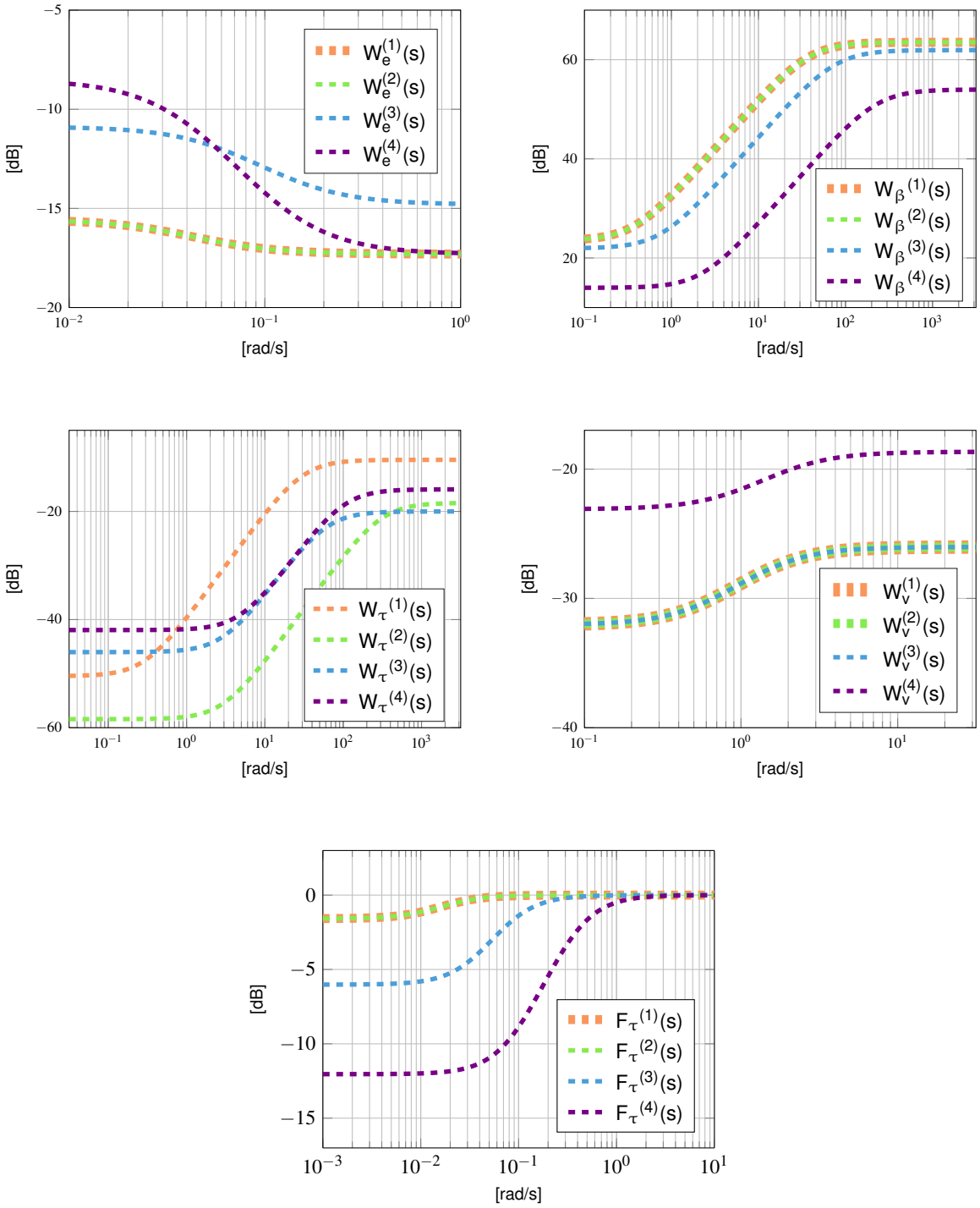

Figure 7. Bode magnitude plots of design weights.

In Region 2, the main objective is to track $\delta\omega_{g\_cmd}$ for maximizing power generation (Objectives 1). W_e is used to specify the tracking performance by limiting the low frequency error with less emphasis on high frequencies. The bandwidth of W_e is $0.04\,\mathrm{rad/s}$ for both $\rho = 6\,\mathrm{m/s}$ and $\rho = 9\,\mathrm{m/s}$, which is slightly larger than the bandwidth of the baseline controller. The coefficient for W_e is 0.15, which indicates relaxed constraints on the sensitivity from $\delta\omega_{g\_cmd}$ to $\delta\tilde{\omega}_e$. This is to balance the performance on rejecting the disturbance $\delta\tilde{v}$. Specifically, the generator speed is allowed to be more sensitive to the

Wind Energ. 2017; **00**:1–18 © 2017 John Wiley & Sons, Ltd.
DOI: 10.1002/we
Prepared using weauth.cls

wind disturbance for capturing more power and relaxing the usage of generator torque. Therefore, the low frequency gain of W_e is also lower in Region 2, as shown in the up-left subplot of Figure 7.

W_τ and W_β are used to penalize actuations of $\delta\tau_g$ and $\delta\beta$, respectively (Objective 5). Both weights are chosen as high pass filters to penalize high frequency control efforts. Here, W_τ has a bandwidth of $0.3\,\mathrm{rad/s}$ at $\rho = 6\,\mathrm{m/s}$ and $3\,\mathrm{rad/s}$ at $\rho = 9\,\mathrm{m/s}$, as the objective of maximizing the power (Objective 1) requires a large variation of torque actuation. The coefficient for W_τ is also relaxed from 0.003 to 0.0012 for more aggressive actuation at $\rho = 9\,\mathrm{m/s}$. The actuation of $\delta\beta$ should be limited in Region 2 to avoid losing power. Therefore, the bandwidth of W_β is limited to $1\,\mathrm{rad/s}$ and the coefficient is set to 30, which indicates a strong penalty.

W_v is used to shape the frequency property of wind disturbance. The power spectrum of wind turbulence usually decays with the high frequency [7]. Therefore, W_v is chosen to be a low pass filter in [7]. However, it is found in the tuning process that this choice of W_v did not have enough emphasis on tower modes (around $2\,\mathrm{rad/s}$) and one of blade edgewise bending modes (around $13\,\mathrm{rad/s}$), which have significant effects on the loads. Therefore, W_v is adjusted to be a high pass filter with slightly higher gain in the high frequency. However, W_v is more relaxed in Region 2 as the requirement for load reduction is less critical.

W_m is used to penalize the bending moments on the tower base (Objective 4). W_m is set to be diagonal assuming no coupling between tower fore-aft and side-to-side motions. The two diagonal entries in W_m are constant in all wind conditions. As the peak gains of 2 tower modes are relatively lower and the weight W_v is relaxed in Region 2, W_m is expected to affect more on the tower loads in Region 3. Therefore, details on W_m will be discussed later.

F_τ is chosen as a high pass filter to restrict the low frequency actuation of $\delta\tau_g$, especially in Region 3. This is to avoid large overshoots of τ_g in high wind speeds. The low frequency gain of F_τ varies with wind speeds and the high frequency gain is $0\,\mathrm{dB}$. As τ_g is the main control input in Region 2, the low frequency gain is around $-1.5\,\mathrm{dB}$ and the turning frequency is around $0.02\,\mathrm{rad/s}$ for both $F_\tau^{(1)}$ and $F_\tau^{(2)}$, which indicate minor penalties.

The objective in Region 2.5 is to ensure a smooth transition of operations (Objective 3). Therefore, these weights are modified to adjust the transition. Specifically, the bandwidth of $W_e^{(3)}$ is extended to $0.1\,\mathrm{rad/s}$ for better tracking. The coefficient of $W_e^{(3)}$ is also tighten to 0.2. As τ_g is close to the rated value in Region 2.5, the coefficient of $W_\tau^{(3)}$ is increased to 0.005 for more penalization. Correspondingly, the coefficient of $W_\beta^{(3)}$ is slightly relaxed and the bandwidth is extended to $2\,\mathrm{rad/s}$. The choice of $W_v^{(3)}$ is the same as in Region 2. As τ_g might increase to the rated value with the turbulence in Region 2.5, it is important to limit the overshoot. Therefore, $F_\tau^{(3)}$ has a low frequency gain of $-6\,\mathrm{dB}$ and the turning frequency is $2\,\mathrm{rad/s}$.

The objective in Region 3 is focused on generator speed tracking and load reduction (Objective 2 and 4). The low frequency gain of $W_e^{(4)}$ is therefore tightened to $-9\,\mathrm{dB}$ and the high frequency gain is relaxed to balance the sensitivity. $W_\tau^{(4)}$ is further penalized to limit the torque actuation, with a coefficient of 0.008. However, the bandwidth of $W_\tau^{(4)}$ is extended to $5\,\mathrm{rad/s}$ and $W_\beta^{(4)}$ is significantly relaxed with a coefficient of 10 and a bandwidth of $6\,\mathrm{rad/s}$. The coefficient of $W_v^{(4)}$ is tightened to 0.7, which indicates higher wind disturbance. As discussed above, the two diagonal entries of W_m are to penalize tower base fore-aft and side-to-side bending moments, respectively (Objective 4). They are chosen based on frequency responses $W_v^{(4)}$ and $G(\rho)$ in Region 3. For example, the peak gain from $\delta\tilde{v}$ to δM_{tfa} is $70\,\mathrm{dB}$ at $\rho = 18\,\mathrm{m/s}$. Therefore, the first diagonal term of W_m is $10^{-3.65}$ such that the peak gain from $\delta\tilde{v}$ to $\delta\tilde{M}_{tfa}$ is smaller than 1. Similar approach is applied to find the second diagonal term of W_m. To further restrict $\delta\beta$, $F_\tau^{(4)}$ has a low frequency gain of $-12\,\mathrm{dB}$ and the turning frequency is $4\,\mathrm{rad/s}$. These settings will ensure less overshoot of τ_g but still allow it to damp out the vibration of high speed shaft at around $13\,\mathrm{rad/s}$, which is introdueced by one of the blade edgewise bending modes.

4.3. Control Synthesis

The LPV toolbox in Matlab [33] is used to synthesize $K(\rho,\dot{\rho})$. One approach is to perform the synthesis with no assumptions on the wind speed acceleration $\dot{v}_{trim}$, i.e. the synthesized controller has no dependence on $\dot{\rho}$. This is known as rate-unbounded design and typically yields conservative results. Thus it is useful to instead perform the synthesis using some physically-motivated bound on $\dot{v}_{trim}$. This design is more computationally demanding but yields less conservative designs. Here the bound is selected as $0.1\,\mathrm{m/s^2}$. This value is calculated by first low-pass filtering a 11 % turbulent wind profile at the wind speed of $20\,\mathrm{m/s}$. The bandwidth of the low pass filter is $0.04\,\mathrm{rad/s}$ which captures the effective wind speed and the resulting signal is considered as v_{trim}. This parameter is further high-pass filtered with a cut-off frequency of $10\,\mathrm{rad/s}$ to get $\dot{v}_{trim}$. The wind profile here is a Class C wind turbulence of IEC 64000-1 standards [43], which corresponds to normal wind conditions.

The choice of a bounded rate requires parameter dependent Lyapunov matrices [19]. For simplicity, an affine dependence is chosen and the calculated upper bound of the induced L_2 norm is close to 1. The computation time is $180\,\mathrm{s}$. As a comparison, an unbounded rate leads to an upper bound of 7.04 and the computation time is $13\,\mathrm{s}$. Figure 8 shows

more synthesis results using different rates with 7 gridding points. Results with 20 gridding points in this figure will be discussed later. It is seen that the upper bound does not increase significantly until $10\,\mathrm{m/s^2}$, which is unrealistic in practice. It indicates that the closed-loop performance is not sensitive to the rate bound (as long as it remains below $10\,\mathrm{m/s^2}$). Therefore, the choice of a bounded rate does lead to a less conservative controller.

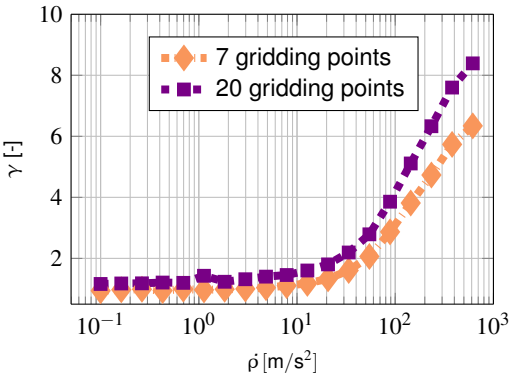

Figure 8. Upper bound of the induced L_2 norm γ with $\dot{\rho}$.

To verify that the choice of 7 gridding points is sufficient for accuracy, a denser gridding set is chosen in increments of $1\,\mathrm{m/s}$ in wind speed from $5\,\mathrm{m/s}$ to $24\,\mathrm{m/s}$, which contains 20 trim points. The synthesis results are also shown in Figure 8. It is noted that the upper bound of the induced L_2 norm is slightly larger than the value with 7 gridding points. However, the computation time is around $700\,\mathrm{s}$. The unbounded parameter varying rate is also considered here. It leads to an upper bound at 9.49 and the time consumption is $41\,\mathrm{s}$. Therefore, the choice of 7 gridding points does not lead to a significant performance degradation and the resulting controller is acceptable for implementation.

As mentioned in Section 1, the LPV control introduced here is different from the commonly used gain scheduling technique. To further quantify the difference, 7 H_∞ controllers are synthesized independently using the weights shown in Table II, which correspond to the 7 gridding points. These controllers are gain-scheduled by linear interpolation, which is similar to the realization of gridded based LPV systems. The LPV toolbox is used to analyze the gain-scheduled controller, by adopting the same assumption on the parameter varying rate and Lyapunov matrices. As a result, the closed loop system is unstable as the induced L_2 norm is infinity. This conclusion is further validated by simulations in FAST. Therefore, the gain-scheduled controller will not be further analyzed or compared with the LPV controller.

4.4. Frequency Analysis

As discussed in Section 4.2, LPV systems do not have a valid frequency interpretation. However, it is still valuable to perform the frequency analysis on some representative frozen trim points. This analysis will be helpful at least on exploring local performance of the LPV controller. It should be noted that $K(\rho,\dot{\rho})$ has a dependence on $\dot{\rho}$. Considering the difficulty on estimating $\dot{\rho}$ and the complexity of implementation, this dependence is ignored by interpolating $K(\rho,\dot{\rho})$ at $\dot{\rho}=0$.

Figure 9 shows frequency responses of the generator speed tracking error $\delta\omega_e\,[\mathrm{RPM}]$ at $\rho = 6\,\mathrm{m/s}$. Here, the LPV controller has slightly better disturbance rejection to $\delta\tilde{v}\,[\mathrm{m/s}]$ in low frequencies. This might lead to less power generation as the low frequency part of wind turbulence also contains energy. However, the power loss will be compensated by lower reference tracking error to $\delta\omega_{g\_cmd}\,[\mathrm{RPM}]$, as shown in the right subplot of Figure 9. As load reduction is not a major concern in Region 2 and the bandwidth of control actuations are limited, frequency responses of the structural loads are similar for the two controllers, which will not be shown.

Frequency responses from $\delta\tilde{v}$ to some selected outputs at $\rho = 18\,\mathrm{m/s}$ are shown in Figure 10. This is a typical wind condition in Region 3 and the objectives are to track the rated generator speed and reduce structural loads. Therefore, the 4 outputs here are the generator speed $\delta\omega_g\,[\mathrm{RPM}]$, high speed shaft torque $\delta\tau_{hss}\,[\mathrm{kN\cdot m}]$, tower base fore-aft bending moment $\delta M_{tfa}\,[\mathrm{kN\cdot m}]$ and side-to-side bending moment $\delta M_{tss}\,[\mathrm{kN\cdot m}]$. As shown in Figure 10, the LPV controller has better disturbance rejection on $\delta\omega_g$ and $\delta\tau_{hss}$. It is noted that the peak on $\delta\tau_{hss}$ is around $13\,\mathrm{rad/s}$ and control actuations with relaxed bandwidth in the LPV design are therefore capable of suppressing this mode. The LPV controller also successfully decreases peaks on δM_{tfa} and δM_{tss}, which are all around $2\,\mathrm{rad/s}$. The load reduction can be attributed to the coordinated actuations of $\delta\tau_g$ and $\delta\beta$ on these structural modes, as shown in Figure 11. As frequency responses at other trim points in Region 3 are similar, it is expected that the LPV controller will reduce more structural loads on the tower and rotor shaft.

Wind Energ. 2017; **00**:1–18 © 2017 John Wiley & Sons, Ltd.
DOI: 10.1002/we
Prepared using weauth.cls

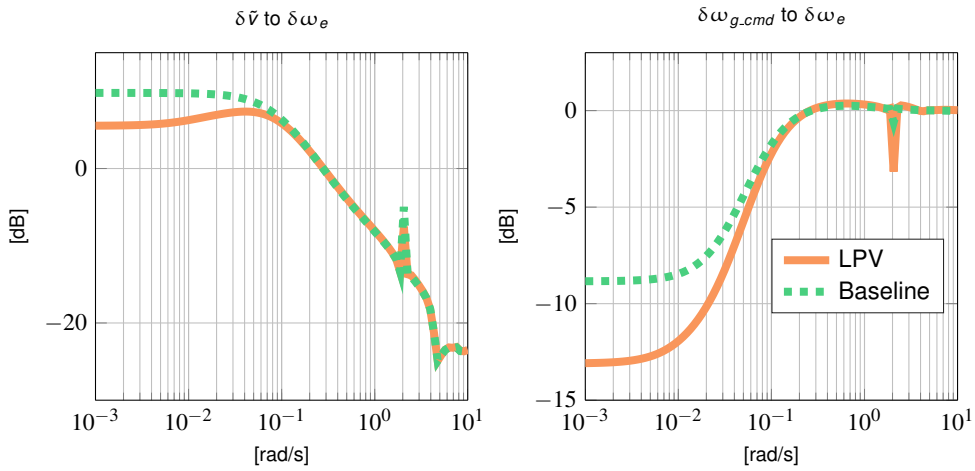

Figure 9. Frequency responses at $\rho = 6\,\mathrm{m/s}$.

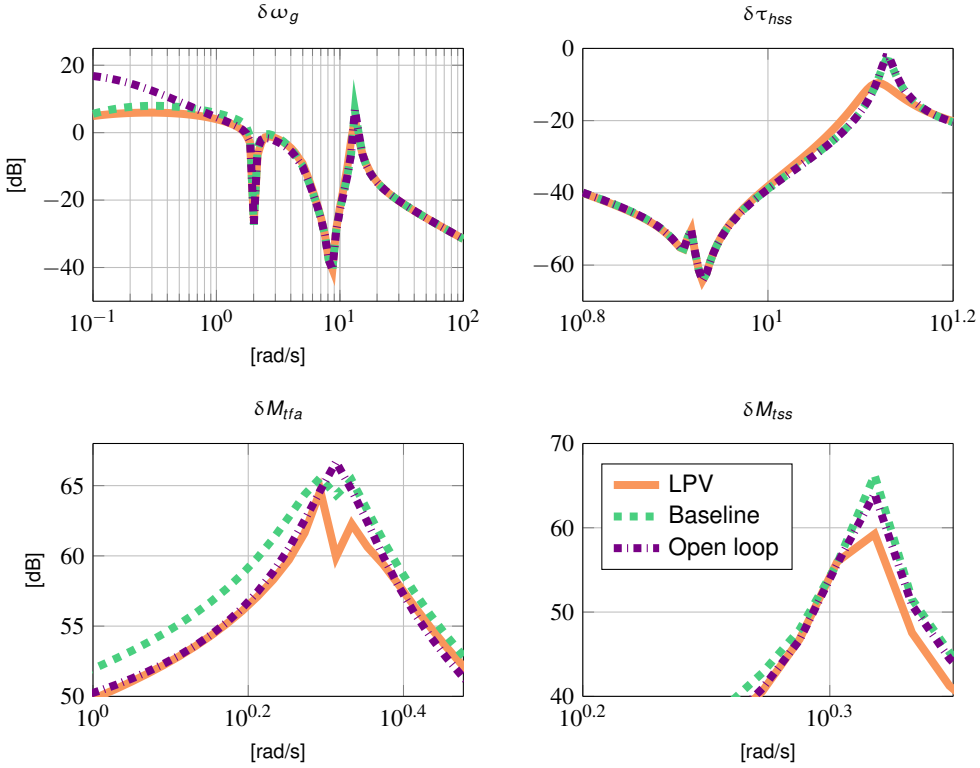

Figure 10. Frequency responses at $\rho = 18\,\mathrm{m/s}$.

To conclude, the LPV controller satisfies performance requirements in different wind conditions. Simulations and post analysis later will show that the frequency analysis is an effective way to predict the performance, which saves time and boosts efficiency in design iterations.

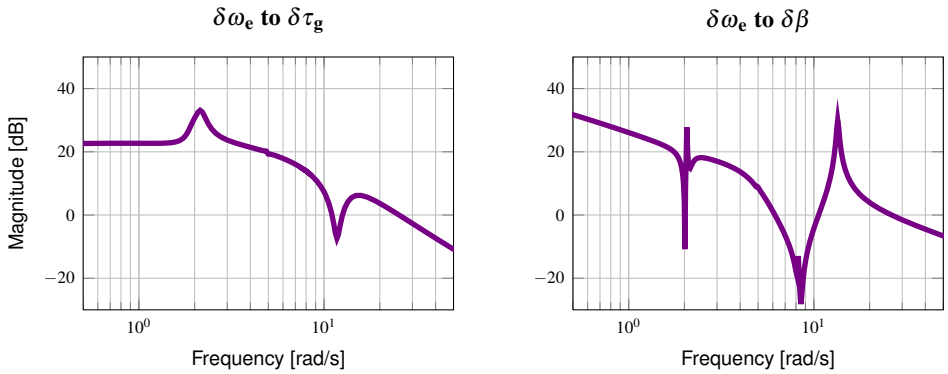

Figure 11. Frequency responses of $K(\rho)$ at $\rho = 18 m/s$.

5. SIMULATIONS AND ANALYSIS

5.1. Simulation Results

The LPV controller and the baseline controller will be compared in FAST. TurbSim [43] is used to generate turbulent wind profiles. The turbulence spectral model is the Kaiman model and the turbulence level is Class C of IEC 64000-1 standards [43], which corresponds to normal wind conditions. The average wind speed ranges from $6\,\mathrm{m/s}$ to $24\,\mathrm{m/s}$ with an increment of $1\,\mathrm{m/s}$. At a specific wind speed, 10 wind profiles will be generated using various seeds and each profile last for $11\,\mathrm{minutes}$. To avoid effects of initial response, however, data collected in the first $1\,\mathrm{minute}$ will be excluded from analysis.

Figure 12 shows simulation results at $\rho = 6\,\mathrm{m/s}$. The hub-height turbulent wind speed and the low pass filtered wind speed estimation are illustrated in the first subplot of Figure 12. The rest subplots compare responses of ω_g, τ_g, β and power P. It is seen that both the two controllers have good generator speed tracking performance. In fact, the LPV controller has a slightly faster actuation of τ_g. However, the extra actuation of β indicates that the weights W_β selected for Region 2 is not tight enough and the power generation could be affected. This is confirmed in Figure 15, which shows that there is an average power loss of $1\,\%$ for all wind profiles at $\rho = 6\,\mathrm{m/s}$ (Objective 1). Results at other wind speeds of Region 2 are similar and will not be shown here.

For simplicity, simulation results at two other wind speeds are shown in Figures 13, which cover Region 2.5 and 3 operations. The time span is limited from $200\,\mathrm{s}$ to $500\,\mathrm{s}$. Subplots at the left column are for $\rho = 12\,\mathrm{m/s}$. Here, both the two controllers try to track ω_{g_rated} and have stable and smooth transition in Region 2.5 (Objective 3). However, their actuations are slightly different. In the LPV controller, specifically, τ_g is allowed to operate around the rated value and therefore goes higher with an increased turbulence. This is shown at around $300\,\mathrm{s}$. While the purpose of using τ_g is to collaborate with β in higher frequency, this overshoot might have side effects to the safety and reliability of the generator. Instead, the baseline controller set τ_g strictly at the rated value for protection. It is also noted that the LPV controller has a slower response from $400\,\mathrm{s}$ to $500\,\mathrm{s}$. This is because τ_g has less emphasis on low frequency responses to $\delta\omega_e$ at $\rho = 12 m/s$. In other words, it has been tuned to focus more on objectives in Region 3, such as damping vibrations on the tower and drive drain which are beyond $2\,rad/s$. The increase of low frequency gain for the torque actuation is gradual as v_{trim} decreases in Region 2.5. This is also the reason why the LPV controller attempts to use more pitch actuations here to track $\delta\omega_{g\_cmd}$. These slightly unbalanced actuations will affect the power generation. However, the power loss is compensated by less structural load on the high speed shaft. The LPV controller attempts to focus more on this load rather than power generation because this load achieves its maximum in Region 2.5. Further details on the load reduction effects will be discussed in Section 5.2.

Simulation results for $\rho = 18\,\mathrm{m/s}$ are shown in subplots at the right column of Figure 13. The generator speed tracking performance are similar for the two controllers. It is calculated that the standard deviation of $\delta\omega_e$ is $30.76\,RPM$ for the baseline controller and $28.70\,RPM$ for the LPV controller (Objective 2). It is noted the LPV controller has more high frequency blade pitch actuations for decreasing the tower and drive train loads. This observation is verified by the power spectral density analysis shown in Figure 14. However, the pitch actuation rolls off quickly beyond $13\,rad/s$ (Objective 5). It is also noted that the baseline controller tries to decrease τ_g for maintaining the rated power generation when ω_g increases too much. This phenomenon happens at around $440\,\mathrm{s}$. While this actuation is helpful to decrease variations of the power generation, it might have some sides effects to the robustness of the system, as it has a tendency to go unstable if the wind speed keeps increasing very fast. In contrast, the LPV controller moderately varies τ_g around the rated value. The range for this variation is adjusted better than at $\rho = 12\,\mathrm{m/s}$ by using a tighter coefficient on the weight W_τ in the design.

Wind Energ. 2017; **00**:1–18 © 2017 John Wiley & Sons, Ltd.
DOI: 10.1002/we
Prepared using weauth.cls

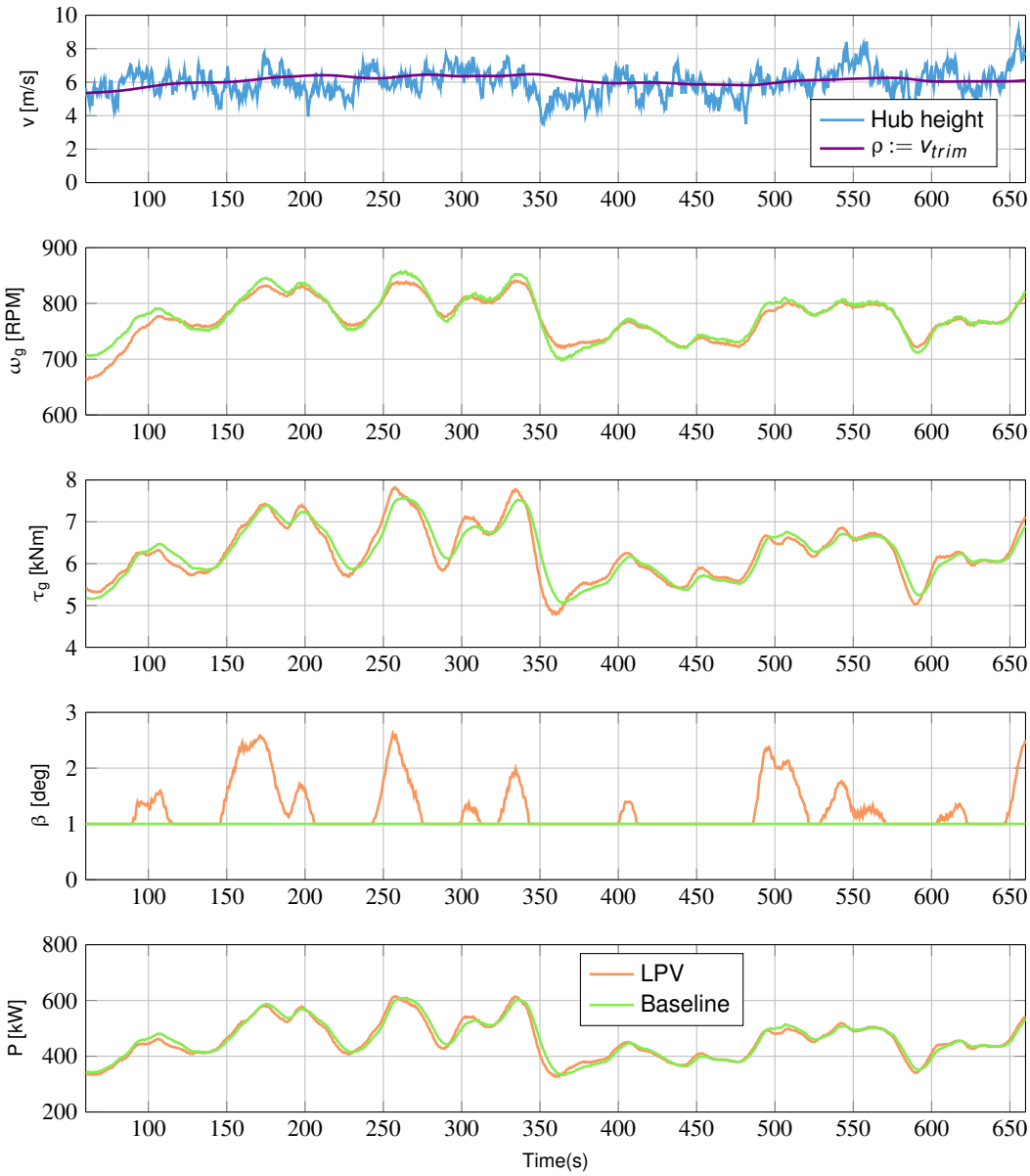

Figure 12. Simulation results at $6\,\mathrm{m/s}$.

5.2. Damage Equivalent Load

For a further comparison between the two controllers, this section provides the damage equivalent loads (DELs) analysis by using the MCrunch [41].

The LPV design is focused on load reductions of the high speed shaft torque τ_{hss}, the tower base fore-aft bending moment M_{tfa} and side-to-side bending moment M_{tss}. The DELs analysis is shown in Figure 16. Here, subplots (a), (c) and (e) show DEL values for the two controllers at 19 wind speeds. Subplots (b), (d) and (f) show percentages of improvement for the LPV controller. It is seen from subplot (a) and (b) that τ_{hss} is almost the same for the two controllers in Region 2, where the requirement for load reduction is not critical. However, τ_{hss} reaches its maximum in Region 2.5. Here the LPV controller shows around 20% improvement. As mentioned in Section 5.1, this comes with the price of around 2 to 3% power loss, which is a trade-off in practice. In region 3, the actuation on τ_g is limited and τ_{hss} is affected more by the high frequency part of the turbulence. It is seen that τ_{hss} keeps increasing with the wind speed for both the two

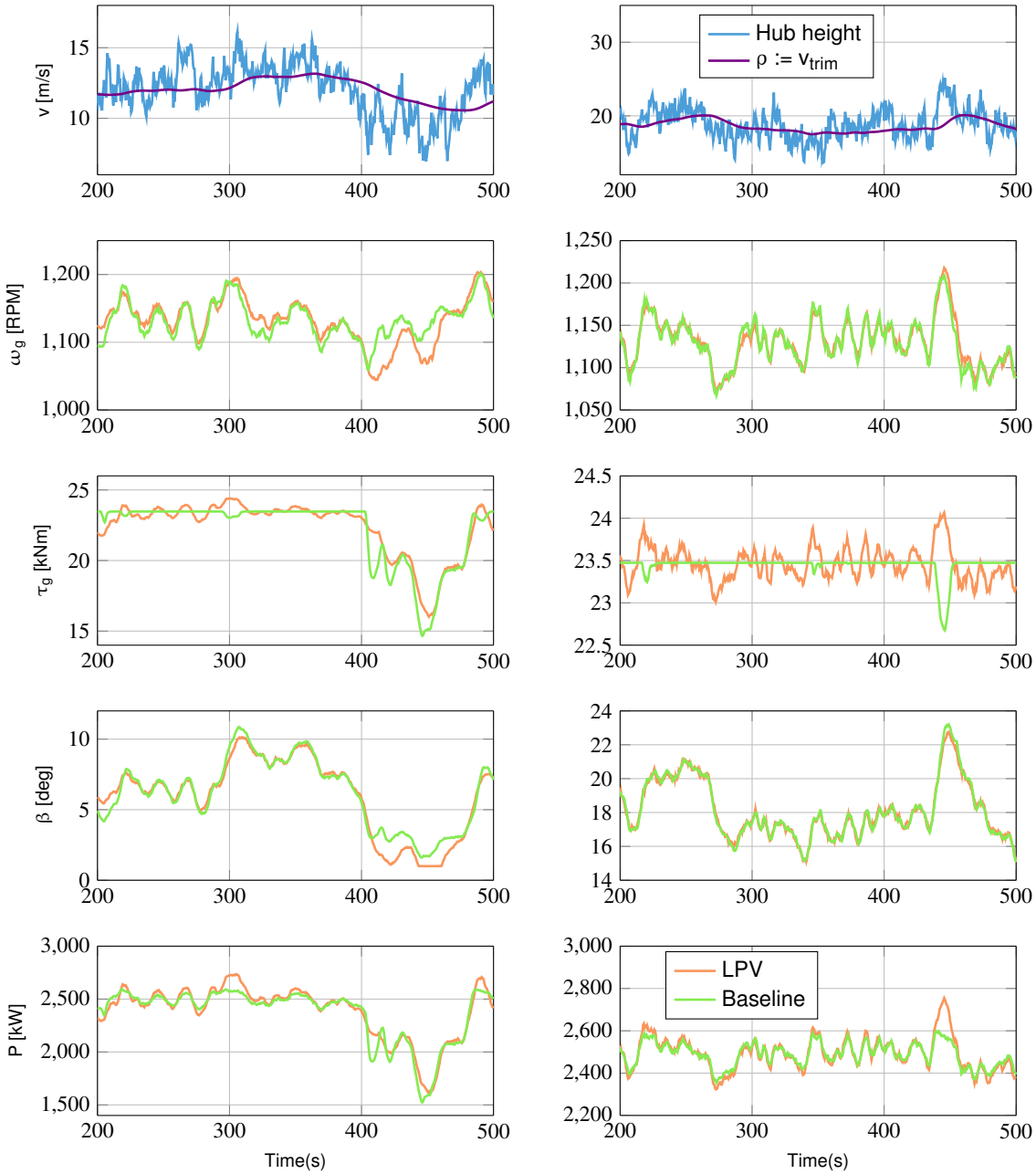

Figure 13. Simulation results at $12\,\mathrm{m/s}$ (left column) and $18\,\mathrm{m/s}$ (right column).

controllers. However, the LPV controller still has around 10 to 20 % improvements until the wind speed goes up to $24\,\mathrm{m/s}$ (Objective 4).

As shown in Figure 16 (c) and (d), the LPV controller has around 10 to 15 % improvement on M_{tfa}, except for Region 2.5 (Objective 4). In fact, the LPV controller increases M_{tfa} by 15 % at $10\,\mathrm{m/s}$. However, it is noted that M_{tfa} reaches its minimum in Region 2.5 for both the two controller. This local degradation should not have a significant effect on the overall performance. The results for the tower side-to-side bending moment are shown in Figure 16 (e) and (f). Generally, M_{tss} has a steady tendency to increase with the wind speed, for both the two controllers. However, the LPV controller successfully decreases the DEL by 40 to 50 % in Region 2.5 and Region 3 (Objective 4). The improvement is less important in Region 2, as M_{tss} is very low here.

Wind Energ. 2017; **00**:1–18 © 2017 John Wiley & Sons, Ltd.
DOI: 10.1002/we
Prepared using weauth.cls

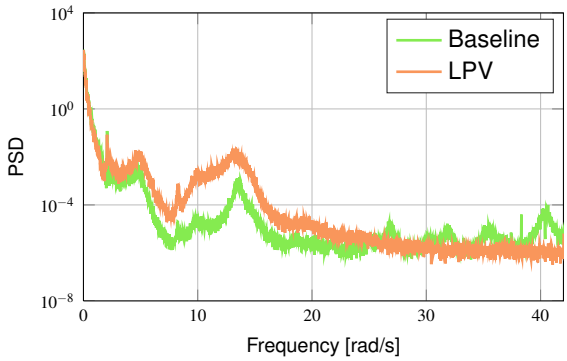

Figure 14. Power spectral densities for blade pitch angles.

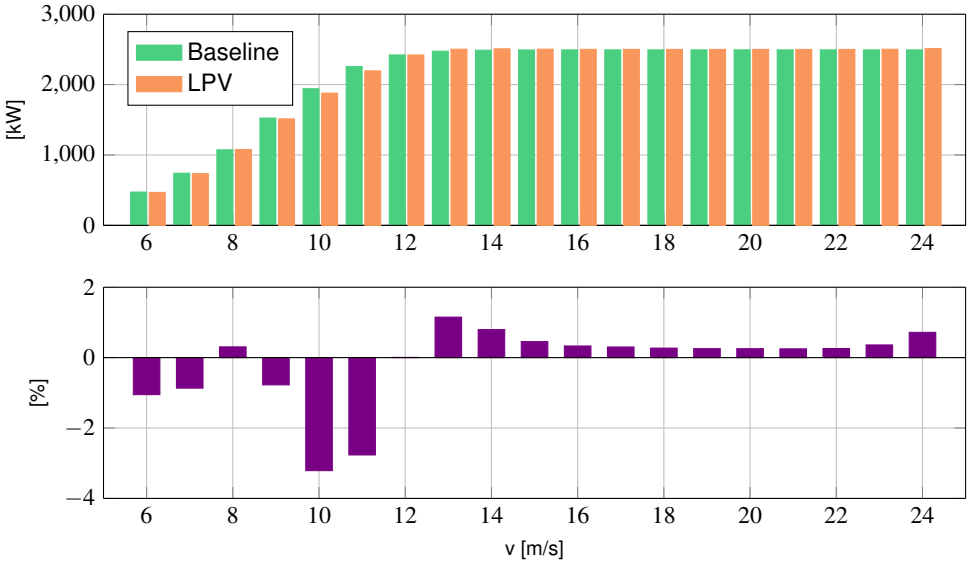

Figure 15. Power generations and the relative loss/increase for the LPV controller.

As individual pitch control is not applied, the LPV controller barely affects the blade loads. For a comprehensive comparison, DELs of the blade flapwise moment M_{bfw} and edgewise moment M_{bew} are shown in Figure 17. Similar to the layout of Figure 16, subplot (a) and (c) show the DEL values for the two moments. Subplot (b) and (d) show percentages of load reduction for the LPV controller. It is seen from Figure 17 (a) and (b) that M_{bfw} generally increases with the wind speed and the two controllers have similar performance, except for several wind speeds of Region 2 and 2.5. The difference between the two controllers is even smaller for M_{bfw}, which indicates minor effects on the blade side-to-side motion.

6. CONCLUSION

This paper proposes an LPV controller for a Clipper wind turbine to operate in all wind conditions. The design is based on a gridded based LPV model of the turbine, which is constructed by interpolation of linearized models at different wind speeds. Details were presented on the design process, such as the model complexity, trade-off of two actuations and choices of parameter varying rate and parameter dependent Lyapunov functions. The proposed LPV controller is able operate the turbine as a classical baseline controller. More importantly, it significantly decreased structural loads on the tower and drive train, by allowing higher bandwidth of actuations. Performance of the LPV controller has been validated at a wide range of wind speeds. Future work will consider limiting the collective blade pitch usage in Region 2 for more power generation and incorporation of individual blade pitch control.

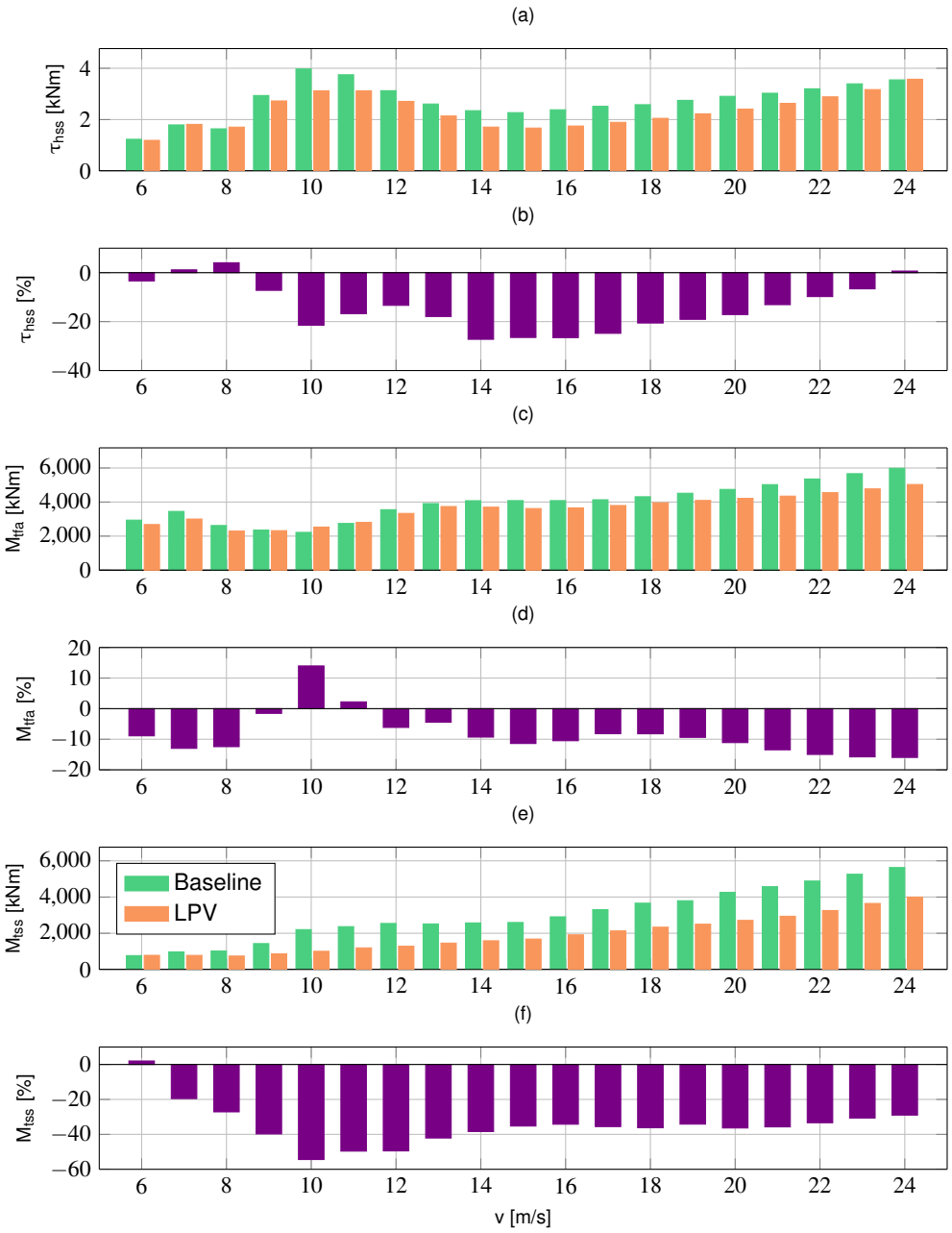

Figure 16. Damage equivalent loads (DELs) on the tower and rotor shaft.

ACKNOWLEDGEMENTS

This work was supported by the Xcel Energy Renewable Energy Fund: Contract No. RD4-13 entitled *Virtual Wind Simulator with Advanced Control & Aeroelastic Model for Improving the Operation of Wind Farms* and the National Science Foundation Grant No. NSF-CMMI-1254129 entitled *CAREER: Probabilistic Tools for High Reliability Monitoring and Control of Wind Farms*.

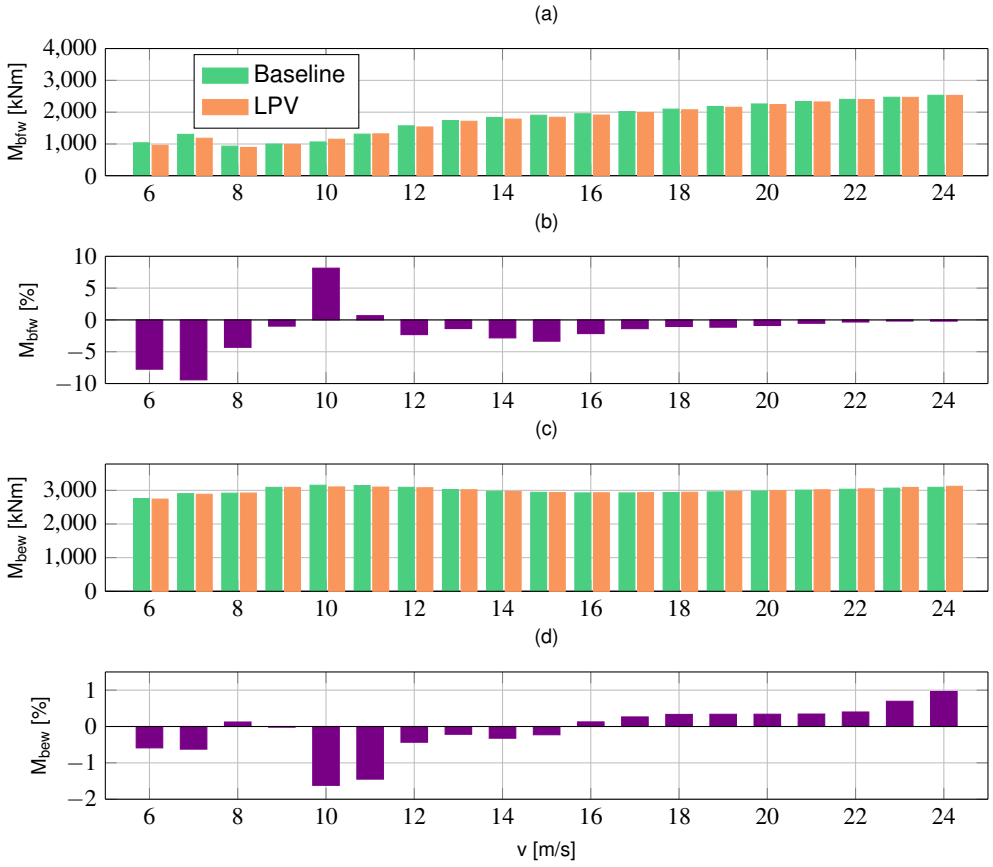

Figure 17. Damage equivalent loads (DELs) on the blades.

REFERENCES

1. Pao LY, Johnson KE. A tutorial on the dynamics and control of wind turbines and wind farms. *American Control Conference*, IEEE, 2009; 2076–2089.
2. Laks J, Pao L, Wright A. Control of wind turbines: Past, present, and future. *American Control Conference*, 2009; 2096–2103.
3. Bossanyi E. The design of closed loop controllers for wind turbines. *Wind Energy* 2000; **3**:149–163.
4. Bossanyi E. Wind turbine control for load reduction. *Wind Energy* 2003; **6**(3):229–244.
5. Bossanyi EA. Individual blade pitch control for load reduction. *Wind Energy* 2003; **6**(2):119–128.
6. Selvam K, Kanev S, van Wingerden J, van Engelen T, Verhaegen M. Feedback–feedforward individual pitch control for wind turbine load reduction. *International Journal of Robust and Nonlinear Control* 2009; **19**(1):72–91.
7. Ozdemir AA, Seiler PJ, Balas GJ. Performance of disturbance augmented control design in turbulent wind conditions. *Mechatronics* 2011; **21**(4):634 – 644.
8. Ossmann D, Theis J, Seiler P. Robust control design for load reduction on a Liberty wind turbine. *ASME Dynamic Systems and Control Conference*, 2016; Paper No. DSCC2016–9719.
9. Ossmann D, Theis J, Seiler P. Load reduction on a Clipper Liberty wind turbine with linear parameter-varying individual blade-pitch control. *Accepted to Wind Energy* 2016; **Vol**(No):x–x.
10. Darrow J, Johnson K, Wright A. Design of a tower and drive train damping controller for the three-bladed controls advanced research turbine operating in design-driving load cases. *Wind Energy* 2011; **14**(4):571–601.
11. Díaz de Corcuera A, Pujana-Arrese A, Ezquerra J, Milo A, Landaluze J. Linear models-based LPV modelling and control for wind turbines. *Wind Energy* 2015; **18**(7):1151–1168.
12. Licari J, Ugalde-Loo CE, Ekanayake JB, Jenkins N. Comparison of the performance and stability of two torsional vibration dampers for variable-speed wind turbines. *Wind Energy* 2015; **18**(9):1545–1559.

13. Fleming PA, Van Wingerden JW, Wright AD. *Comparing state-space multivariable controls to multi-siso controls for load reduction of drivetrain-coupled modes on wind turbines through field-testing*. American Institute of Aeronautics and Astronautics (AIAA), 2012.
14. Østergaard KZ. Robust, gain-scheduled control of wind turbines. PhD Thesis, Automation and Control, Department of Electronic Systems, Aalborg University 2008.
15. Bianchi FD, De Battista H, Mantz RJ. Robust multivariable gain-scheduled control of wind turbines for variable power production. *International Journal of Systems Control* 2010; **1**(3).
16. Inthamoussou FA, Bianchi FD, De Battista H, Mantz RJ. LPV wind turbine control with anti-windup features covering the complete wind speed range. *Energy Conversion, IEEE Transactions on* 2014; **29**(1):259–266.
17. Apkarian P, Gahinet P. A convex characterization of gain-scheduled H_∞ controllers. *IEEE Trans. on Automatic Control* 1995; **40**:853–864.
18. Wu F. Control of linear parameter varying systems. PhD Thesis, University of California, Berkeley 1995.
19. Wu F, Yang XH, Packard A, Becker G. Induced $\mathscr{L}_2$ norm control for LPV systems with bounded parameter variation rates. *International Journal of Robust and Nonlinear Control* 1996; **6**:983–998.
20. Hoffmann C, Werner H. A survey of linear parameter-varying control applications validated by experiments or high-fidelity simulations. *Control Systems Technology, IEEE Transactions on* 2015; **23**(2):416–433.
21. Bianchi F, Mantz R, Christiansen C. Control of variable-speed wind turbines by LPV gain scheduling. *Wind Energy* 2004; **7**(1):1–8.
22. Østergaard KZ, Stoustrup J, Brath P. Rate bounded linear parameter varying control of a wind turbine in full load operation. *IFAC Proceedings Volumes* 2008; **41**(2):5593–5598.
23. Østergaard KZ, Stoustrup J, Brath P. Linear parameter varying control of wind turbines covering both partial load and full load conditions. *International Journal of Robust and Nonlinear Control* 2009; **19**(1):92–116.
24. Bianchi FD, De Battista H, Mantz RJ. Robust multivariable gain-scheduled control of wind turbines for variable power production. *International Journal of Systems Control* 2010; **1**(3).
25. Bobanac V, Jelavić M, Perić N. Linear parameter varying approach to wind turbine control. *14th International Power Electronics and Motion Control Conference*, 2010; T12–60–T12–67.
26. Bakka T, Karimi HR, Christiansen S. Linear parameter-varying modelling and control of an offshore wind turbine with constrained information. *Control Theory & Applications, IET* 2014; **8**(1):22–29.
27. Sloth C, Esbensen T, Stoustrup J. Robust and fault-tolerant linear parameter-varying control of wind turbines. *Mechatronics* 2011; **21**(4):645–659.
28. Adegas FD, Sonderby IB, Hansen MH, Stoustrup J. Reduced-order LPV model of flexible wind turbines from high fidelity aeroelastic codes. *Control Applications (CCA), 2013 IEEE International Conference on*, IEEE, 2013; 424–429.
29. Shirazi FA, Grigoriadis KM, Viassolo D. An integrated approach towards structural and LPV controller design in wind turbines. *American Control Conference (ACC), 2012*, IEEE, 2012; 5789–5794.
30. Apkarian P, Adams R. Advanced gain-scheduling techniques for uncertain systems. *IEEE Trans. on Control Systems Technology* 1998; **6**(1):21–32.
31. Packard A. Gain scheduling via linear fractional transformations. *Systems & Control Letters* 1994; **22**(2):79–92.
32. Jonkman J, Buhl M. *FAST User's Guide*. National Renewable Energy Laboratory, Golden, Colorado 2005.
33. Hjartarson A, Seiler P, Packard A. LPVTools: A toolbox for modeling, analysis, and synthesis of parameter varying control systems. *IFAC-PapersOnLine* 2015; **48**(26):139–145.
34. Eolos wind energy research consortium. Http://www.eolos.umn.edu/.
35. Burton T, Sharpe D, Jenkins N, Bossanyi E. *Wind Energy Handbook*. 1st edn., John Wiley & Sons, 2001.
36. Bir GS. User's guide to MBC3: Multi-blade coordinate transformation code for 3-bladed wind turbine 2010; .
37. Østergaard KZ, Brath P, Stoustrup J. Estimation of effective wind speed. *Journal of Physics: Conference Series*, vol. 75, IOP Publishing, 2007; 012 082.
38. Mikkelsen T, Hansen K, Angelou N, Sjöholm M, Harris M, Hadley P, Scullion R, Ellis G, Vives G. Lidar wind speed measurements from a rotating spinner. *Proc. European Wind Energy Conference, Warsaw, Poland*, 2010.
39. Johnson K, Pao L, Balas M, Fingersh L. Control of variable-speed wind turbines: standard and adaptive techniques for maximizing energy capture. *IEEE Control System Magazine* 2006; **26**(3):70–81.
40. Wang S, Seiler P. Gain scheduled active power control for wind turbines. *AIAA Atmospheric Flight Mechanics Conference*, 2014; Paper No. AIAA–2014–1220.
41. M Buhl J. Mcrunch user's guide for version 1.00 May 2008. Http://www.nrel.gov/docs/fy08osti/43139.pdf.
42. Zhou K, Doyle J, Glover K. *Robust and Optimal Control*. Prentice-Hall, 1996.
43. Jonkman BJ. Turbsim user's guide: Version 1.50 2009.

DOI: 10.1002/we
Prepared using weauth.cls